Stabilization of a turbulent premixed flame by a plasma filament

Kong, Chengdong; Li, Zhongshan; Aldén, Marcus; Ehn, Andreas

Published in:
Combustion and Flame

DOI:
10.1016/j.combustflame.2019.07.002

2019

Document Version:
Publisher's PDF, also known as Version of record

Combustion and Flame 208 (2019) 79–85

Contents lists available at ScienceDirect

Combustion and Flame

journal homepage: www.elsevier.com/locate/combustflame

Stabilization of a turbulent premixed flame by a plasma filament

Chengdong Kong*, Zhongshan Li, Marcus Aldén, Andreas Ehn

Division of Combustion Physics, Lund University, P.O. Box 118, SE-221 00 Lund, Sweden

ARTICLE INFO

Article history:
Received 12 January 2019
Revised 11 March 2019
Accepted 1 July 2019
Available online 10 July 2019

Keywords:
Plasma assisted combustion
Turbulent flame stabilization
Spatial separation
Atmospheric-pressure discharge
Laser diagnostics

ABSTRACT

The mechanism of stabilizing a turbulent premixed methane-air flame using warm filamentary plasma is investigated by using laser diagnostics. First, stabilization of a turbulent jet flame is demonstrated in a setup using a pin-to-pin plasma discharge. The coupled plasma-flame structures were visualized utilizing planar laser-induced fluorescence (PLIF) of formaldehyde (CH_2O) and methylidyne radicals (CH), as well as laser Rayleigh scattering thermometry imaging. The results show that the plasma channel and the flame front are spatially separated by a layer of hot burning products attributed to the flame propagation from the plasma core. Because of this spatial separation, the impacts of plasma on combustion are primarily thermal since the energetic radical species (such as O, H), produced by the discharge, have short equilibration time and cannot spread far away from the discharge channel before reaching the equilibrium state. From this point of view, turbulence would be beneficial for promoting the transport of plasma-produced radicals and thus bridge the gap between the plasma and the flame front. The plasma is still able to stabilize the flame. Based upon the experimental results, a frequent ignition-flame propagation (FIFP) model is proposed to explain the flame stabilization process. For the contracted plasma filament, the local power density is high enough to initialize the flame kernel that propagates away from the plasma channel until extinction. The propagation process is, however, strongly affected by turbulence. Local extinction is highly probable and thus the flame front has to be close to the ignition source at strong turbulence. At such conditions, the stabilized flame can be regarded as a large number of flame pockets, repeating the three phases of ignition, propagation and extinction, which can be summarized as the FIFP model. It infers that the flame propagation phase is important for sustaining the flame to complete combustion. Hence, this phase should be extended, which is more probable to achieve if the plasma ignition pilot is located in a section of limited turbulence.

1. Introduction

Flame stabilization at extreme conditions is a crucial issue for power conversion using combustion devices. The general ideas to stabilize a turbulent flame are to enhance flame speed through chemical kinetics and control the flow field. The bluff body and swirling flows are common schemes to create low velocity zones and increase the local residence time for flame stabilization. On the other hand, reactant preheating, exhaust gas recirculation and pilot flames are schemes to enhance chemical reaction rates [1,2]. In the recent decades, plasma, especially the non-thermal plasma, has been proposed as a potential scheme to stabilize and even control combustion due to its short response time and the ability to stabilize combustion processes [3]. Discharge can be produced in a gas by applying high voltage between two electrodes. Deposition of electrical energy through plasma in the combustion system can produce active species and heat, as well as modify transport processes. Positive effects of plasma on the flame stabilization have been confirmed by numerous experimental studies [4–6].

The effects of plasma on combustion can be divided into three fundamental subjects, i.e. chemical kinetics, transport and thermal effect [3]. Plasma enhanced reaction kinetics have been widely studied [7–15]. In general, due to the presence of plasma, various excited species and new reaction pathways are created. As for the transport, the plasma can change the local diffusivity by decomposing the fuel or oxidant molecules to small fragments [3], or produce ionic wind [16,17] and hydrodynamic instabilities [18] to modify the local flow field and mixing. The modification of local flow field by plasma directly impacts the flame propagation and stabilization behaviors [19–21]. The temperature increment by plasma can directly accelerate the chemical reactions following the

* Corresponding author.
E-mail addresses: honestkong@sina.com, chengdong.kong@forbrf.lth.se (C. Kong).

https://doi.org/10.1016/j.combustflame.2019.07.002

Arrhenius law. Even though these isolated effects have been extensively investigated, challenges still remain. The main challenge comes from the complexity of the physicochemical coupling and the spatial heterogeneity. On the one hand, the aforementioned enhancement pathways are coupled together and render it arduous to determine the controlling mechanism during the plasma assisted combustion. On the other hand, the real flame is generally spatially inhomogeneous and the discharge is inclined to be filamentary at the atmospheric pressure or higher. It means that the direct interaction between the flame front and the plasma becomes difficult owing to the non-uniform characteristics of discharge and combustion. It is of fundamental interests to understand how the flame and the discharge interact and couple in a realistic high-pressure, turbulent combustion system.

In order to clarify the interactions between filamentary plasma and flame, simultaneous visualization of plasma and flame during plasma assisted combustion is necessary. Up to now, related work is still scarce. One example is the measurement of the hydroxyl (OH), methylidyne (CH), and formaldehyde (CH_2O) profiles during a nanosecond discharge between two needles in the CH_4-air mixture by Grisch et al. [22]. In our recent work, a gliding arc assisted turbulent flame was investigated to demonstrate the flame-plasma structure [23].

In this article, we aim to explore the interaction between plasma and flame and thus understand the mechanism of filamentary plasma assisted flame in a turbulent jet flow. The plasma was generated by a pin-to-pin discharge setup with an alternating current (AC) power supply. Compared to other plasma sources, such as dielectric-barrier discharge (DBD), corona discharge and nanosecond pulsed discharge, the plasma column produced here is more trackable and has longer time to interact with flow and flame. Furthermore, this gliding arc discharge is warm and should be more efficient to sustain the real turbulent flame. Methane-air mixtures were fed into the discharge volume by a jet flow. Ignition and flame propagation processes were studied by visualizing the flame-discharge structures with the laser diagnostic techniques (including CH, CH_2O PLIF and Rayleigh scattering techniques). The role of turbulence in coupling the plasma and the flame is analyzed based upon the equilibration time of crucial radical species. Finally, the stabilization mechanism is discussed.

2. Experimental setup

Figure 1 shows a schematic of the experimental setup. Air and methane were mixed and ejected into open air through a long stainless steel pipe, forming a jet flow. In order to change the turbulence intensity with a limited flow rate, two pipes with inner diameters (I.D.) of 1.5 mm and 4 mm, respectively were used. The I.D. 4 mm pipe is default in this article. The I.D. 1.5 mm pipe was used to generate a high turbulent flow if needed. Two tungsten needles, positioned about 1 cm above the exit of the pipe, were used as electrodes for discharge. These tungsten needles with a diameter of 1.6 mm were bought from BGRIMM Advanced Materials Science & Technology Co., Lth. Their tip-to-tip gap distance was 0.8 cm. One electrode was connected to a 35 kHz AC power supply (Generator 9030 E, SOFTAL Electronic GmbH), whereas the other electrode was grounded. In order to protect the electrodes and control the discharge, the power supply was set to burst mode [24], which is explained by the inset of Fig. 1. The duration of a high voltage burst (i.e. t_{on}) and the delay time between bursts (i.e. t_{off}) can be independently controlled by a pulse generator (BNC 575, Berkeley Nucleonics Corp.). During the laser based measurements, the repetition rate of the high-voltage burst was set to 10 Hz to synchronize with the laser pulse. The rated power of the high-voltage supply can be manually set instead of current and voltage. It means that the current and the voltage change depending on the length

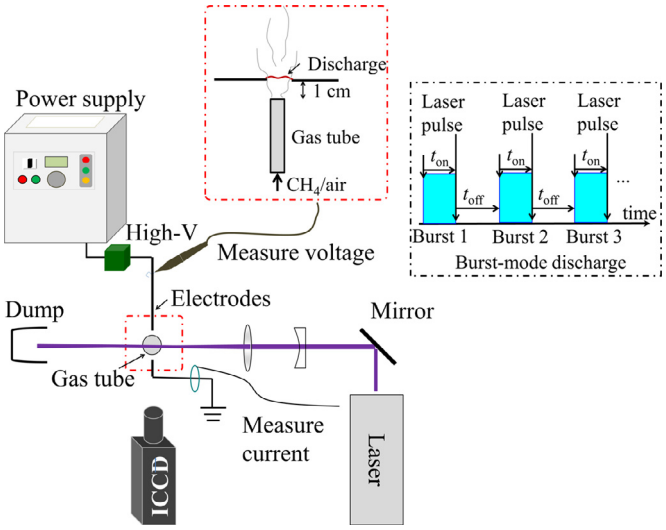

Fig. 1. Schematic of the experimental setup. Insets show the side view of the tube burner and the electrodes, as well as the synchronization of the discharge bursts and the laser pulses.

of the discharge column and the energy dissipation rate around the plasma column [25]. A current monitor (Pearson Electronics) and a voltage probe (Tektronix P6015A) were employed to measure the waveforms of the current (I) and the voltage (U) simultaneously, thus to understand the realistic electrical characteristics of the studied discharge.

PLIF of CH/CH_2O and Rayleigh scattering measurements were performed to detect the radical and translational temperature profiles. The CH PLIF measurement was conducted using an Alexandrite laser (101-PAL, Light Age Inc.) tuned to 383.3 nm for CH excitation [26]. A Brilliant B Nd: YAG laser (Quantel) with the second and third harmonic units was employed to generate a 355 nm laser beam for the excitation of CH_2O. The Rayleigh scattering measurement was conducted using the second harmonics of a Brilliant B pulsed Nd: YAG laser (Quantel). PI Max II ICCD cameras (Princeton Instruments) equipped with visible Nikon lens and appropriate filters (434 ± 8.5 nm interference filter for CH_2O and GG 400 long-pass filter for CH, 532 ± 5 nm interference filter for Rayleigh scattering) were used to acquire the CH/CH_2O/Rayleigh signals. In the Rayleigh scattering thermometry, the absolute temperature can be determined by comparison with a reference gas target, following a relationship given by [27].

$$T_{tgt} = \frac{I_{ref}}{I_{tgt}} \times T_{ref} \times \bar{\sigma}_{tgt}/\bar{\sigma}_{ref} \quad (1)$$

where T_{tgt} is the unknown target temperature; T_{ref} is the known temperature of the reference target; I_{tgt} and I_{ref} are the Rayleigh scattering signals from the detected target and the reference target, respectively; $\bar{\sigma}_{tgt}$ and $\bar{\sigma}_{ref}$ are the averaged Rayleigh cross sections of the detected target and the reference, respectively. Usually, the room temperature air is chosen as the reference target to calculate the absolute temperature of detected target. The main uncertainties of Rayleigh scattering thermometry include the stray light from background and the chemical compositions in the plasma column. Usually the uncertainty of chemical compositions in plasma is neglected [28]. The gaseous composition in the post-flame zone can be estimated according to the equivalence ratio with the assumption of complete reaction. The stray light is difficult to estimate but we know that with the stray light intensity increase, the measured temperature drops. It means that the measured temperature value is underestimated. In the experiment, the laser and the high-voltage power supply are both controlled and synchro-

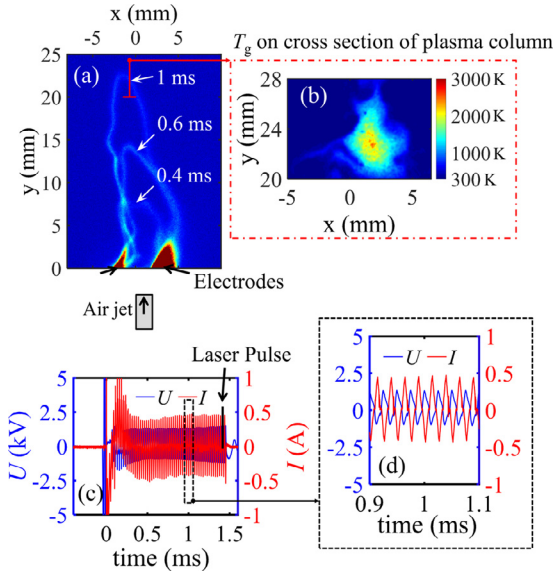

Fig. 2. (a) Image of the overlaid filamentary plasma columns (ICCD gate: 600 ns; Three single-shot images captured at 0.4 ms, 0.6 ms and 1 ms are overlaid); (b) Single-shot translational temperature profile captured at a discharge time of 1.4 ms. (c) Current and voltage waveforms during the discharge; (d) Rescaled current-voltage waveforms to indicate the oscillating current and voltage. The current is inversely plotted to be distinguished from the voltage.

nized by using the BNC pulse generator. The discharge time (i.e. t_{on}), the delay time between high-voltage bursts (i.e. t_{off}) and the laser pulse timing were adjusted to make sure that the laser pulse was fired at the discharge time of t_{on}, as indicated in the inset of Fig. 1. By varying t_{on}, the detected signal intensity as a function of discharge time can be acquired and analyzed. The current and voltage signals together with the ICCD gates were simultaneously recorded using a four-channel oscilloscope (PicoScope 4424, PS) at a sample rate of 2 GHz.

3. Results and discussion

3.1. Characteristics of a pin-to-pin discharge

A filamentary plasma column in the pure air without fuel was generated between two needle electrodes. The typical discharge image and the temperature profile on the cross section of the plasma column, together with current and voltage waveforms are shown in Fig. 2. In this case, the flow rate is 18 standard liter per minute (SLPM) and the corresponding Reynolds number is around 7000 at the room temperature of 298 K. The measured current and voltage waveforms indicate that when the high voltage is applied to initiate the discharge, current spike always occurs. After the initial breakdown stage, the discharge transits to a glow discharge stage with relatively low current and voltage. The glow regime is basically confirmed by the estimation of cathode fall. During this stage, the plasma column moves downstream driven by flow and elongates. The diameter of the discharge column is around 0.6 mm estimated from the spontaneous emission. The peak current value is 420 mA at the glow discharge stage. The length of plasma column at a discharge time of 1 ms reaches around 6 cm and the voltage amplitude is 1.3 kV for the case in Fig. 2. Hence, the average electric field strength in the plasma channel is estimated to be 22 kV/m. The input electrical power is around 6.5 kW per meter of plasma column. The translational temperature profile around the plasma column is measured using the Rayleigh scattering thermometry, as shown in Fig. 2(b). The peak translational temperature in the plasma column is in the range of 2000 K to 2500 K. The size of the hot region (>1500 K) is 3–4 mm, which is much larger than the diameter of the plasma column. Provided a temperature of 2300 K, the reduced electric field strength (E/N) can be estimated to be 7 Td. The mean electron energy can reach 0.8 eV (9283 K) calculated by using the Bolsig+ Boltzmann solver [29]. It means that the gas temperature is still much lower than the electron temperature and thus the plasma column is non-equilibrium. The cases with the addition of methane and flame show similar discharge characteristics around the plasma column. Since the initial breakdown accompanies too strong emissions to interfere with measurements, the results shown in the below sections are all acquired at the glow discharge stage.

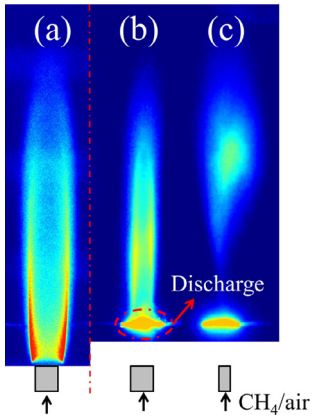

Fig. 3. Flame images without and with plasma discharge present. The exposure time of camera is 1/40 s. (a) Self-sustained laminar flame, (b) Discharge stabilized laminar flame, (c) Discharge stabilized turbulent flame.

3.2. Demonstrations of a filamentary plasma stabilized jet flame

The flame images captured by a digital single-lens reflex camera (Nikon D7200) is illustrated in Fig. 3 to show the impacts of plasma discharge on flame structures. An interference filter (434 ± 8.5 nm) was used in acquiring the spontaneous flame emissions from CH (A-X) transitions and at the same time blocking other useless signals from background. The flow rate and the turbulence intensity were varied for different flame stability. In Fig. 3(a), the jet flow rate is 1.1 SLPM, corresponding to a *Re* number of 424 and thus the flame can be self-sustained without discharge. As the flow rate increases, the flame cannot be self-sustained but blow off. However, with the assistance of a pin-to-pin discharge, the flame is stabilized, as shown in Fig. 3(b-c). The discharge is in the burst mode with a burst duration time of 1 ms and a burst repetition frequency of 100 Hz. Here two flame shapes are detected under different flow conditions. In Fig. 3(b), the flow rate is 2.0 SLPM and the *Re* number is 757, indicating a laminar flow. Therefore, the flame shape is similar to a typical self-sustained laminar flame except that the flame is anchored on the plasma volume. While in Fig. 3(c), a pipe burner with the inner diameter of 1.5 mm was used to increase the turbulence. The flow rate is 2.5 SLPM and the *Re* number reaches 2550. This is basically a turbulent flow and thus the flame shape is quite different compared to that in Fig. 3(b).

3.3. Structure of filamentary plasma assisted flame

The laser-based diagnostic techniques were applied to visualize the instantaneous plasma-flame structure. Here the temperature profile was measured by Rayleigh scattering thermometry to indicate the high-temperature region. CH_2O PLIF was carried out to visualize the preheat zone and the low temperature region. PLIF

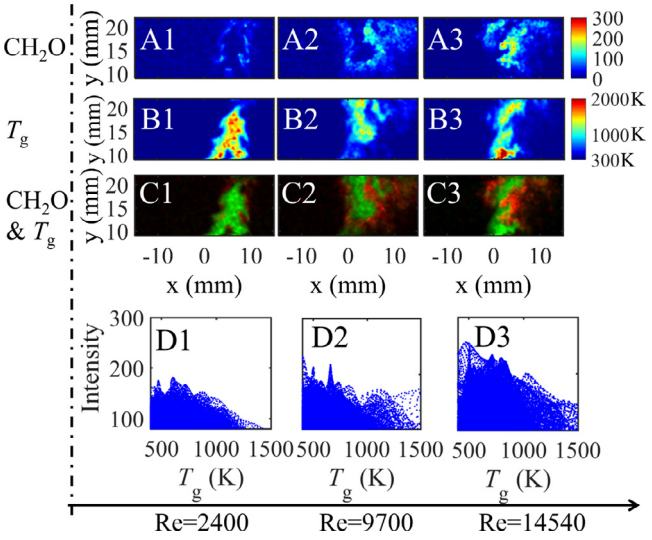

Fig. 4. Simultaneous measurement of temperature (T_g) and CH_2O PLIF signal profiles. A: CH_2O; B: T_g; C: the overlaid temperature and CH_2O profile; D: the pixel-to-pixel statistical correlations between the local CH_2O intensity and the temperature (T_g). The numbers 1, 2 and 3 denote three flow conditions with *Re* numbers of 2400, 9700 and 14540.

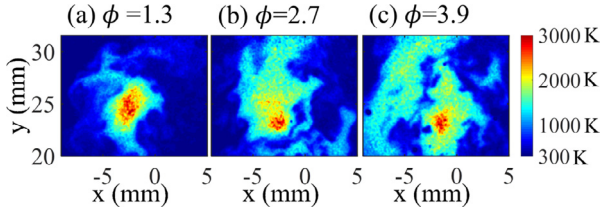

Fig. 5. Translational temperature distributions with varying nominal equivalent ratio (ϕ). In these images, the red region with temperature higher than 2000 K is the plasma core. (For interpretation of the references to color in this figure legend, the reader is referred to the web version of this article.)

of CH was conducted to mark the flame front. All the images are single-shot.

Figure 4 illustrates the simultaneously measured single-shot temperature and relative PLIF CH_2O signal intensity distributions under different flow rate conditions with the *Re* number increase from 2400 to 14,540. The pipe burner with an inner diameter of 1.5 mm was used. These images were captured at the discharge time of 2 ms. The nominal equivalent ratio (ϕ), which is calculated from the flow rates of CH_4 and air, is 2.7. Due to the entrainment of surrounding air, the real ϕ should be lower than the nominal value. Figure 4A displays the CH_2O profile whereas Fig. 4B shows the temperature profile. Overlaid temperature and CH_2O profile is displayed in Fig. 4C. Figure 4D shows pixel-to-pixel statistical correlations between the local CH_2O intensity and the temperature (T_g). In Fig. 4, the flame downstream the plasma was acquired without the plasma column included in the images. The result confirms that the CH_2O is hard to survive in the hot region ($T_g > 1500$ K) but spread widely in the low-temperature region from 400 K to 1000 K. Furthermore, with the turbulence intensity increased, the CH_2O distribution becomes wider and more penetrated into the hot region. The increased spreading of CH_2O can be due to the turbulent transport of CH_2O since the CH_2O has a relatively long lifetime, but also possibly the transport of long-lived radicals generated by the plasma column, that can produce CH_2O from CH_4.

Figure 5 shows the single-shot translational temperature distributions during plasma assisted combustion, with varying nominal equivalent ratio (ϕ). The signal is acquired at the discharge

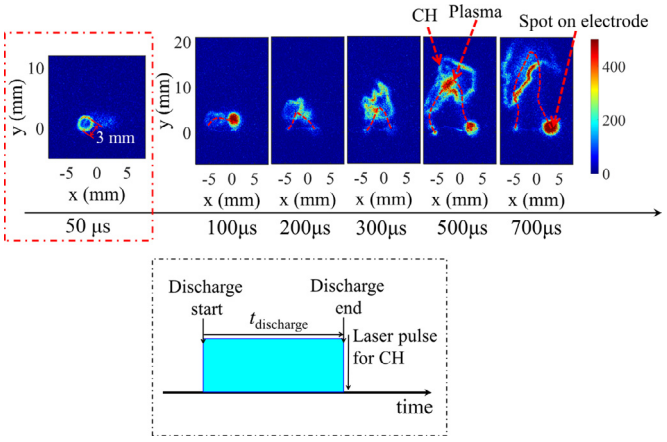

Fig. 6. CH profiles as a function of the discharge duration time. The red dashed line represents the plasma channel. Inset shows the synchronization of discharge and laser pulse. (For interpretation of the references to color in this figure legend, the reader is referred to the web version of this article.)

time of 1.5 ms. The small pipe burner (I.D. 1.5 mm) was used and the flow rate was 9.4 SLPM, with the *Re* number of 9700. By comparing the temperature in Figs. 2 and 4, it indicates that the temperature of post flame zone is in the range of 1500 to 2000 K while the peak temperature of the discharge column is between 2000 K and 3000 K. Thus the gas volume that is affected by the plasma column can be distinguished from the flame region that is virtually unaffected by the plasma according to the temperature profiles. As demonstrated in Fig. 5, the high-temperature plasma core is localized in a 3–4 mm wide region while the hot post-flame region is found away from the plasma core. The post-flame region is further broadened with increased nominal ϕ. It implies that the flame front can propagate further away from the plasma column with an increased nominal ϕ without being extinguished.

The spatial separation between the plasma column and the flame front can be further confirmed from the CH PLIF measurement. During this measurement, the discharge time and the laser pulse timing were controlled by the BNC pulse generator to acquire the CH profiles after a certain moment of discharge, as indicated in the inset of Fig. 6. The laser pulse was fired just when the discharge was switched off. Single-shot CH PLIF signal profiles as a function of the discharge time are shown in Fig. 6. The flow rate was 16.2 SLPM, the nominal ϕ was 1.85 and the *Re* number was 6260. The emissions from the electrode tips and the plasma column are too strong to be totally blocked by the long-pass filter and the time-gated ICCD camera with a gate time of 150 ns and are thus still visible in these figures. Nevertheless, the CH distributions can be recognized in the image since it is a thin layer and not spatially overlapping with the plasma luminescence. In Fig. 6, the CH profile at 50 μs was captured with a smaller laser sheet so the length scale of image at 50 μs is different from the other images. It is manifested that the flame front in the discharge assisted flame is several millimeters away from the plasma column. Similar results were previously obtained where a gliding arc discharge was used to support a turbulent flame [23]. Since the thin CH ring with a size of 3 mm is detected 50 μs after the discharge starts, it infers that around the plasma column the ignition delay must be shorter than 50 μs. As the discharge time increases, the plasma column elongates driven by the jet flow. Meanwhile, the flame front expands and propagates, closely following the plasma column until the high-voltage burst is turned off or a new plasma column is regenerated between the electrodes.

According to the CH_2O/CH PLIF and Rayleigh scattering measurements, the basic flame-plasma structure is summarized in Fig. 7. The discharge plasma channel defines the center of this

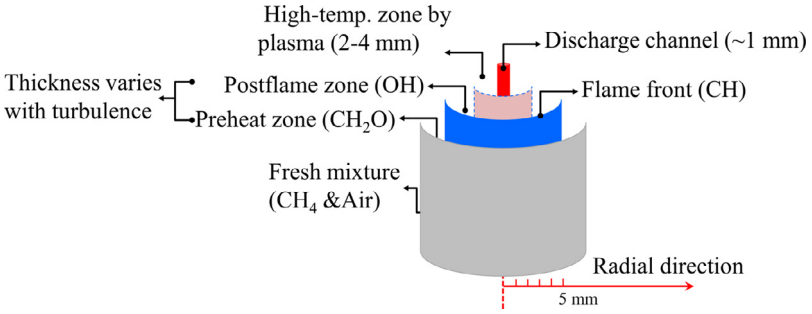

Fig. 7. Schematic of the flame-plasma structure, including the discharge channel in the center, the high-temperature zone due to the plasma, the post flame zone, the flame front, the preheat zone and fresh mixture.

geometry, which is surrounded by an inner 2–4 mm wide high temperature region with a temperature of around 2000 K to 3000 K. This high-temperature discharge region is surrounded by a second high-temperature region (i.e. post-flame zone) with slightly lower temperature (1500–2000 K). The CH-layer, which can be seen as the flame front, is located around this outer high-temperature region. Previous results indicate that OH radicals fill in the gap between the discharge column and the flame front [23] and should thus overlap with the two high-temperature regions. The width of the outer high-temperature region changes depending on the local burning conditions where it increases due to the flame propagation but shrinks when the local extinction dominates. Outside the flame front is the preheat zone, which is seen by the CH_2O PLIF signal. Due to the turbulent transport of active radicals, CH_2O can be detected far away from the flame front.

3.4. Interaction between filamentary plasma and flame front

Experiments have confirmed the spatial separation between the plasma column and the flame front. The reason for this spatial separation is that the plasma column is sustained by the external input, while the flame front must propagate against the flame product for self-sustaining. Owing to this different propagation characteristic, the spatial separation of the flame front and the plasma column is inevitable. The separation rate is determined by the local flame propagation speed and thermal expansion. Figure 6 indicates a separation time of 0.7 ms for a gap distance of 5 mm. It infers a propagation speed of flame front to be roughly 5.7 m/s. This huge propagation speed is largely attributed to the gas thermal expansion around the plasma column. Assuming a constant pressure and the temperatures varying from 300 K to 2000 K across the flame front, the corrected flame speed can be estimated to be 0.8 m/s, which is still larger than the laminar flame speed of methane. Nevertheless, as the flame front moves away from the plasma column, the flame propagation speed should diminish to the normal value unaffected by plasma.

As schematically shown in Fig. 8, the non-thermal plasma column and the flame front are separated by a near-equilibrium post-flame zone. In the plasma column, the radical species have concentrations deviated from the chemical equilibrium due to the continuous collisions between energetic electrons and molecules. However, outside the plasma column, without the excitation of energetic electrons, the radical concentrations could decay to equilibrium. It is important to estimate the distance over which the non-equilibrium plasma can impact and thus evaluate the kinetic effect of plasma on flame. This can be reduced to a problem with radical transport, mixing and equilibration. Through the estimation of the transport and mixing speed and the equilibration time, the affected distance by plasma can be obtained. Since different radical species have different time scales to reach equilibrium, some important radical species for combustion should be chosen. Usually,

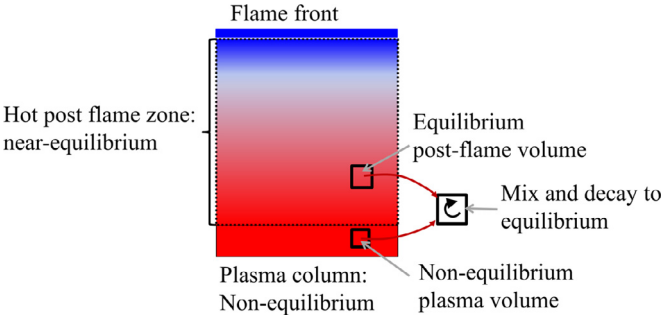

Fig. 8. Schematic of mixing and equilibrating of the radicals from the non-equilibrium plasma and the equilibrium post-flame zone.

the main radicals for enhancing combustion at high temperature by plasma include O, H and OH. Therefore, the equilibration time of those radicals in the post-flame zone are evaluated. We admit that in the plasma, the electronically excited species are always produced. Nevertheless, the lifetime of excited species is shorter than the non-excited one and outside the plasma column they can be quickly quenched at high pressure. Therefore, for simplicity, we only consider the non-excited species. Before estimating the equilibration time of radicals, the initial non-equilibrium chemical compositions should be determined. Here the non-equilibrium chemical composition in the plasma column is approximated by assuming that it is close to the chemical equilibrium state with an increased effective temperature (e.g. 4500 K) [30]. Specifically, the temperature of a CH_4-air mixture with ϕ equal to 1 is increased to the effective temperature (4500 K) and let the gas mixture equilibrate. Then this equilibrated mixture is quenched to a low temperature (e.g. 1500 K and 2000 K), with the chemical composition fixed. Since the equilibrium temperature has changed, the created gas mixture is non-equilibrium and used to represent the warm plasma here. The post-flame gas composition can be easily obtained by equilibration. Those two gas volumes are mixed and decay using a zero-dimensional constant-pressure-temperature reactor to estimate the equilibration time. Here the simulations were performed using the open-source Cantera solver (version 2.3.0) [31].

Figure 9 shows the decay curves of the radical species (including H, O and OH) at temperatures of 1500 K and 2000 K. In the simulation, the proportion of non-equilibrium plasma volume is set to 1%. Under the chosen conditions, the active radicals (i.e. H and O) decay rapidly within hundreds of microseconds. At a typical postflame temperature of 1500 K, the decay time scale of H and O is around 100 μs. Assuming a diffusivity of 10^{-4} m^2/s and a diffusion time of 100 μs, the diffusion length is only 0.1 mm. Therefore, those radicals can be nearly equilibrated close to the plasma column. On the other hand, since the turbulent mixing time scale can be of the order of hundreds of microseconds, turbulence

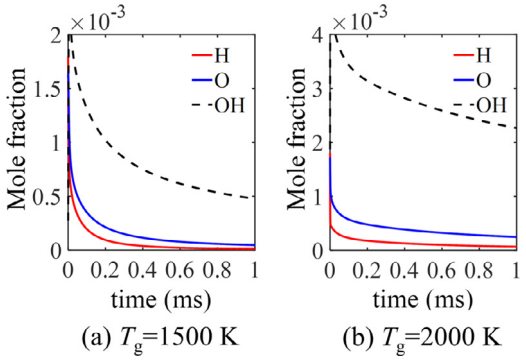

Fig. 9. Decay curves of radical species (i.e. H, O and OH) at temperatures of (a) 1500 K and (b) 2000 K.

might assist the transport of short-lived radicals. Therefore, turbulence can work as a bridge to couple the plasma and the flame front kinetically. OH has an extended lifetime at higher temperatures, which increase the possibilities of plasma-produced OH to stimulate the combustion processes with assistance of turbulence.

In all, the spatial separation between the flame front and the plasma column hinders the direct interaction of plasma and flame and the active non-equilibrium radicals could approach the equilibrium states when crossing the gap. It means that the kinetic effect becomes weaker and the thermal effect is more dominating. However, the turbulence could make potential impacts to bridge the plasma and the flame since the turbulent transport scale is similar to the radical lifetime scale.

3.5. Discussion on the turbulent flame stabilization by plasma columns

Generally, extinction of a turbulent flame occurs when the fuel-oxidant mixture does not have enough residence time to achieve complete combustion. So, the common methods to prevent extinction include enhancement of the chemical reaction rates and prolongation of the residence time. Besides, additional input of external energy sources is another approach to prevent extinction and stabilize flame. The external energy source such as the discharge column has been confirmed to stabilize a turbulent jet flame, as shown in Fig. 3. The mechanism for this flame stabilization can be explained by a frequent ignition-flame propagation model (FIFP). As schematically illustrated in Fig. 10, a burst plasma source is localized near the burner nozzle. When the fuel/oxidant flows into the discharge region, the fresh fuel would be ignited to form a flame kernel, which moves downstream with the flow and propagates until extinction. When the fuel/oxidant mixture experiences the ignition, propagation and extinction phases repetitively, a global turbulent flame is sustained. Therefore, the stabilized turbulent flame can be regarded as a large number of flame pockets, repeating the ignition, propagation and extinction processes. For a semi-quantitative discussion, some parameters are introduced in Fig. 10. u_f denotes an effective flow speed; u_{prop} denotes an effective flame propagation speed; f_{dis} represents the repetition frequency of discharge bursts; t_{flame} represents the effective lifetime of flame pocket ignited by a single burst discharge; l_f is the traveled distance of flame pocket between the discharge bursts; l_{prop} is the downstream propagated distance of flame pocket within its lifetime; l_{flame} is the distance between the plasma source and the end of flame pocket. Provided that the interaction between flame pockets ignited by different discharge burst is neglected, l_{flame} can be estimated as the product of u_f and t_{flame}. It implies that a short lifetime of flame pockets results in a small flame volume, while a long lifetime of flame pockets results in a large flame volume and also high combustion efficiency. By comparing l_f and l_{prop}, the interaction between the flame pocket and the plasma source can be analyzed. If l_f is larger than l_{prop}, the flame pocket and the discharge initialized by the next high-voltage burst are spatially separated and thus there is no burst-to-burst interaction. However, if l_f is smaller than l_{prop}, the flame pocket and the next burst discharge are partially overlapping. Therefore, the burst discharge and the combustion are coupled together and it is believed that some synergetic effect could work to promote each other. Since l_f is inversely proportional to f_{dis}, a larger f_{dis} can promote the couplings of flame pockets and burst discharges. Detailed investigations need to be done in the future and are not discussed further.

An energy enhancement factor (η_p) is introduced in order to quantify the efficiency of the plasma for turbulent combustion promotion. This factor is defined as the ratio of overall combustion-released power (P_{comb}) to the plasma input power (P_e), that is necessary for sustaining the flame (see Eq. (2)).

$$\eta_P = P_{comb}/P_e \tag{2}$$

When the plasma source is filamentary, the plasma input power (P_e) can be expressed by Eq. (3),

$$P_e = I \times E \times l_p \tag{3}$$

where I is the current through the plasma channel, E is the electric field strength inside the plasma, l_p is the length of the plasma channel. The combustion power of a stabilized turbulent flame is estimable with Eq. (4).

$$P_{comb} = S_T \times A_f \times \Delta H \tag{4}$$

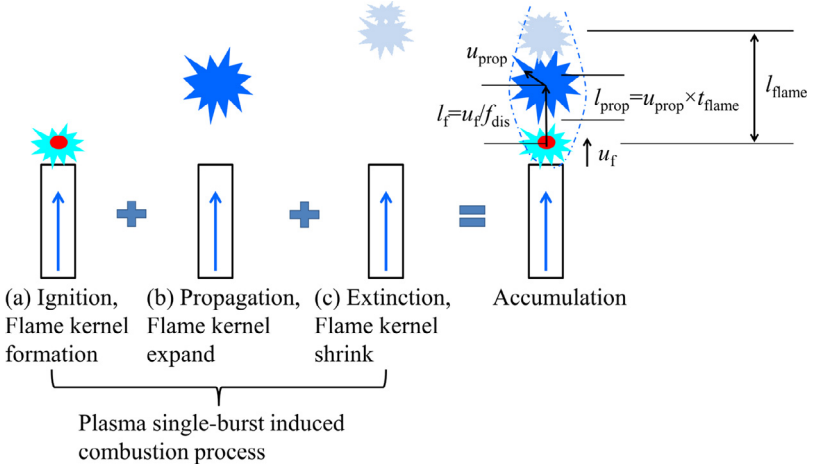

Fig. 10. Schematic of a frequent ignition-flame propagation model.

Where S_T is the effective turbulent flame speed, A_f is the averaged flame area and ΔH is the energy release rate per cubic meter fresh gas.

According to the above definition, when the flame is self-sustained, the value of η_p becomes infinite since P_e is zero. Whereas, when the flame needs to be externally sustained, η_p is limited. We consider an extreme case to estimate the lower limit of η_p. In an extremely turbulent flow, the flame can only be sustained around the plasma column. By assuming that the flame front is 3 mm away from the plasma center, the effective turbulent flame speed is 10 times the laminar flame speed, and the equivalence ratio is 1, P_{comb} is estimated to be 164 kW per meter of plasma column. P_e is 6.5 kW/m when the average current is 0.29 A and the electric field strength is 22 kV/m. Hence η_p is estimated to be 25.

For a practical burning system, the larger η_p is better. Usually expansion of the flame area is a good way to increase η_p. The FIFP model implies that the plasma only works in the ignition as well as the initial propagation stages. Afterwards, the flame kernels need self-sustained until extinction. Therefore, the flame area is mainly determined by the free flame propagation after the plasma forced ignition. So to promote the flame propagation, the plasma assistance should be combined with the traditional schemes for flame stabilization (e.g. bluff body, swirling flow). As an example, it is better to put the plasma source upstream of the large vortexes, and the flame can thus propagate further downstream.

4. Conclusion

We have investigated the stabilization mechanism of turbulent flame by a filamentary plasma discharge. The results confirm that a turbulent jet flame can be sustained by a pin-to-pin discharge. The plasma-flame structure was visualized using the laser-based diagnostics. A spatial separation between the plasma and the flame front is verified. The underlying mechanism is owing to the different propagation characteristics of plasma and flame. Because of this spatial separation, the impacts of plasma on combustion can mainly be interpreted as a thermal effect, since the energetic radical species like O, H have short lifetimes and cannot spread far away from the plasma column. Hence, from this point of view, turbulence could be beneficial to promote the radical transport and bridge the discharge and combustion.

A frequent ignition-flame propagation model (FIFP) is proposed to explain the flame stabilization under an atmospheric turbulent condition. Generally, at the atmospheric pressure, the plasma is inclined to be contracted into filament, where the local energy density is large enough for the fuel/oxidant mixture ignition and flame kernel formation. These flame kernels move with the flow and propagate outwards until extinction. Continuous ignition-flame propagation-extinction processes result in a stabilized turbulent flame. According to this model, the flame propagation phase is important to improve the efficiency of plasma assistance and should be extended. So the plasma source is better to be placed in the locations where the flame can propagate further, such as the recirculation zones.

Acknowledgments

The work was financially supported by Swedish Energy Agency (225383, 389131), Swedish Research Council (2015-05321), Knut and Alice Wallenberg foundation (2015.0294), and European Research Council through the advanced grant TUCLA (669466).

References

[1] M.K. Bobba, Flame stabilization and mixing characteristics in a stagnation point reverse flow combustor, Georgia Institute of Technology, 2007.
[2] X. Pradip, Investigation of flame stabilization mechanisms in a premixed combustor using a hot gas cavity-based flame holder, Normandie University, 2015.
[3] Y.G. Ju, W.T. Sun, Plasma assisted combustion: dynamics and chemistry, Prog. Energy Combust. Sci. 48 (2015) 21–83.
[4] W. Kim, H. Do, M.G. Mungal, M.A. Cappelli, A study of plasma-stabilized diffusion flames at elevated ambient temperatures, IEEE Trans. Plasma Sci. 36 (2008) 2898–2904.
[5] M.S. Bak, H. Do, M.G. Mungal, M.A. Cappelli, Plasma-assisted stabilization of laminar premixed methane/air flames around the lean flammability limit, Combust. Flame 159 (2012) 3128–3137.
[6] G. Pilla, D. Galley, D.A. Lacoste, F. Lacas, D. Veynante, C.O. Laux, Stabilization of a turbulent premixed flame using a nanosecond repetitively pulsed plasma, IEEE Trans. Plasma Sci. 34 (2006) 2471–2477.
[7] M. Uddi, N. Jiang, I.V. Adamovich, W.R. Lempert, Nitric oxide density measurements in air and air/fuel nanosecond pulse discharges by laser induced fluorescence, J. Phys. D: Appl. Phys. 42 (2009) 075205.
[8] S. Nagaraja, V. Yang, Z.Y. Yin, I. Adamovich, Ignition of hydrogen-air mixtures using pulsed nanosecond dielectric barrier plasma discharges in plane-to-plane geometry, Combust. Flame 161 (2014) 1026–1037.
[9] S. Nagaraja, T. Li, J.A. Sutton, I.V. Adamovich, V. Yang, Nanosecond plasma enhanced $H_2/O_2/N_2$ premixed flat flames, Proc. Combust. Inst. 35 (2015) 3471–3478.
[10] T. Ombrello, S.H. Won, Y.G. Ju, S. Williams, Flame propagation enhancement by plasma excitation of oxygen. Part I: effects of O_3, Combust. Flame 157 (2010) 1906–1915.
[11] W.T. Sun, S.H. Won, T. Ombrello, C. Carter, Y.G. Ju, Direct ignition and S-curve transition by in situ nano-second pulsed discharge in methane/oxygen/helium counterflow flame, Proc. Combust. Inst. 34 (2013) 847–855.
[12] S.M. Starikovskaia, A.Y. Starikovskii, D.V. Zatsepin, Hydrogen oxidation in a stoichiometric hydrogen-air mixture in the fast ionization wave, Combust. Theor. Model. 5 (2001) 97–129.
[13] S.A. Bozhenkov, S.M. Starikovskaia, A.Y. Starikovskii, Nanosecond gas discharge ignition of H_2 and CH_4 containing mixtures, Combust. Flame 133 (2003) 133–146.
[14] S.M. Starikovskaia, Plasma-assisted ignition and combustion: nanosecond discharges and development of kinetic mechanisms, J. Phys. D: Appl. Phys. 47 (2014) 353001.
[15] A.C. DeFilippo, J.Y. Chen, Modeling plasma-assisted methane-air ignition using pre-calculated electron impact reaction rates, Combust. Flame 172 (2016) 38–48.
[16] M. Belhi, P. Domingo, P. Vervisch, Modelling of the effect of DC and AC electric fields on the stability of a lifted diffusion methane/air flame, Combust. Theor. Model. 17 (2013) 749–787.
[17] S.H. Won, M.S. Cha, C.S. Park, S.H. Chung, Effect of electric fields on reattachment and propagation speed of tribrachial flames in laminar coflow jets, Proc. Combust. Inst. 31 (2007) 963–970.
[18] Y.H. Ren, W. Cui, S.Q. Li, Electrohydrodynamic instability of premixed flames under manipulations of dc electric fields, Phys. Rev. E 97 (2018) 013103.
[19] S.H. Yoon, S. Bohyeon, J. Park, S.H. Chung, M.S. Cha, Edge flame propagation via parallel electric fields in nonpremixed coflow jets, Proc. Combust. Inst. 37 (2019) 5537–5544.
[20] J. Kuhl, G. Jovicic, L. Zigan, A. Leipertz, Transient electric field response of laminar premixed flames, Proc. Combust. Inst. 34 (2013) 3303–3310.
[21] Y.H. Ren, S.Q. Li, W. Cui, Y.Y. Zhang, L. Ma, Low-frequency AC electric field induced thermoacoustic oscillation of a premixed stagnation flame, Combust. Flame 176 (2017) 479–488.
[22] F. Grisch, G.A. Grandin, D. Messina, B. Attal-Tretout, Non-Equilibrium kinetic studies of plasma-assisted combustion using laser-based diagnostics, Z Phys. Chem. 225 (2011) 1193–1205.
[23] J.L. Gao, C.D. Kong, J.J. Zhu, A. Ehn, T. Hurtig, Y. Tang, S. Chen, M. Alden, Z.S. Li, Visualization of instantaneous structure and dynamics of large-scale turbulent flames stabilized by a gliding arc discharge, Proc. Combust. Inst. 37 (2019) 5629–5636.
[24] Z.W. Sun, J.J. Zhu, Z.S. Li, M. Alden, F. Leipold, M. Salewski, Y. Kusano, Optical diagnostics of a gliding arc, Opt. Express 21 (2013) 6028–6044.
[25] C.D. Kong, J.L. Gao, J.J. Zhu, A. Ehn, M. Alden, Z.S. Li, Characterization of an AC glow-type gliding arc discharge in atmospheric air with a current-voltage lumped model, Phys. Plasmas 24 (2017) 093515.
[26] Z.S. Li, J. Kiefer, J. Zetterberg, M. Linvin, A. Leipertz, X.S. Bai, M. Alden, Development of improved PLIF CH detection using an alexandrite laser for single-shot investigation of turbulent and lean flames, Proc. Combust. Inst. 31 (2007) 727–735.
[27] S.F. Adams, J.E. Caplinger, B.S. Sommers, Spatial temperature mapping of an atmospheric microdischarge using ultraviolet rayleigh scatter imaging, Plasma Sources Sci. Technol. 24 (2015) 025031.
[28] J.J. Zhu, A. Ehn, J.L. Gao, C.D. Kong, M. Alden, M. Salewski, F. Leipold, Y. Kusano, Z.S. Li, Translational, rotational, vibrational and electron temperatures of a gliding arc discharge, Opt. Express 25 (2017) 20243–20257.
[29] G.J.M. Hagelaar, L.C. Pitchford, Solving the boltzmann equation to obtain electron transport coefficients and rate coefficients for fluid models, Plasma Sources Sci. Technol. 14 (2005) 722–733.
[30] C.D. Kong, J.L. Gao, J.J. Zhu, A. Ehn, M. Alden, Z.S. Li, *Re*-igniting the afterglow plasma column of an AC powered gliding arc discharge in atmospheric-pressure air, Appl. Phys. Lett. 112 (2018) 264101.
[31] https://sourceforge.net/projects/cantera/.